

# Effect of zinc addition on the tribological behavior of aluminum-based close-cell metal foams

Ankur Bisht<sup>1</sup>, Brijesh Gangil<sup>1\*</sup>, Vinay Kumar Patel<sup>2</sup>, Sandeep Kumar<sup>1</sup>

<sup>1</sup>*Department of Mechanical Engineering, S.O.E.T., H.N.B. Garhwal University Srinagar, Garhwal 246174, Uttarakhand, India*

<sup>2</sup>*Department of Mechanical Engineering, Govind Ballabh Pant Institute of Engineering and Technology, Pauri Garhwal-246194, India*

Received 4 March 2022, received in revised form 24 August 2022, accepted 1 December 2022

## Abstract

Metal foams are a unique material that is gaining attraction in various industries due to their multifunctional features. This work focuses on understanding the tribological behavior of aluminum-based close-cell metal foams where Zn is added as reinforcement in different weight percentages (0, 0.5, and 1 wt.%). Dry sliding wear tests are performed at varying loads (5, 10, 15, and 20 N) and sliding distances (1000, 2000, 3000, and 4000 m). During the tests, two limiting conditions are considered: the sliding speed of the rotating disc and its track diameter, which are set at  $2.5 \text{ m s}^{-1}$  and 10 cm, respectively. The result reveals that specific wear rate (SWR) is a function of porosity, which increases with an increase in porosity. It was discovered that wear occurs when asperities of varying hardness come into contact at lower stress levels. However, at greater load values, the mechanism shifts from abrasion to plastic flow and delamination.

**Key words:** metal foam, specific wear rate (SWR), SEM

## 1. Introduction

Cellular materials already exist in nature, imparting different structural and functional applications; some materials developed are wood, bones, etc. The development of synthetic cellular foams starts with producing polymeric foams, which are very popular worldwide. With increasing interest, metals and alloys are also converted into foams to find suitability in various structural and functional applications [1–4]. Metals and alloys with controlled porosity are used in various fields depending upon their porosity. Metal foams with closed-cell structures are helpful for structural applications, while open-cell metal foams are valuable for functional applications. Lightweight materials with good strength are beneficial in the automotive, naval, and aerospace industries. Using other properties, they also want to make heat exchangers, silencers, fire stoppers, filters, bulletproof jackets, heat radiators, structured templates and supports, electrode muffling devices, etc. [5–8].

Ayoub Mirzaei et al. [9] used  $\text{CaCO}_3$  as a blowing agent and calcium granules as a thickening agent to produce Al metal foam. The best values for Ca and  $\text{CaCO}_3$  are 1.5 and 1 wt.%, respectively. Tong Shi et al. [10] produced 6063 aluminum alloy and pure aluminum foam through the melt route method. The materials were tested for microstructural and compression behavior. They concluded that 6063 Al alloy foam possesses higher compression strength than pure Al metal foam. M. Heldari Ghaleh [11] developed A356 close-cell Al foam without a stabilizing agent. The results reveal that it is possible to produce aluminum metal foam without a stabilizing agent with equal physical and mechanical properties. D. Yang et al. [12] prepared ex-situ aluminum cellular structure-filled tubes. The samples were tested for quasi-static compression and energy absorption behavior, and it was reported that the filling ratio and positioning of the cellular structure inside the tube play a crucial role in tailoring the foam's compression and energy absorption behavior. G. Timac et al. [13] prepared Ni-718

---

\*Corresponding author: e-mail address: [brijeshgangil@gmail.com](mailto:brijeshgangil@gmail.com)

super alloy foam through the space holder technique. In this technique, carbamide space holders were used to produce foam. The investigation was based on determining the effect of space holder particles on the density and porosity of the samples. The results show that porosity increases with the percentage of a space holder. E. Linul et al. [14] investigated the mechanical behavior of metal foams at a higher temperature. The study shows that as temperature goes up, compressive stress and energy absorption go down, but the plateau region gets longer. J. Kovacik et al. [15] prepared close-cell Zn foam through the powder metallurgy method with porosity ranging from 78 to 91 %. The deformation behavior of Zn foam was similar to that of Al foam, but there was a significant decrement in the compression strength of Zn foam at a similar density. Aluminum metal foam has gained enormous interest among researchers trying to improve the mechanical properties of foams by different means. One way to improve the mechanical properties is by adding reinforcing particles inside the melt during manufacturing. Xia et al. [16] added Mn particles to the melt to improve mechanical and physical properties. Ankur Bisht et al. [17] added Zn and Mg particles in varying percentages to obtain better physical and mechanical properties. Plenty of work has been reported on enhancing mechanical properties, so it is good to observe another dimension of metal foams. Amit Vishwakarma [18] added cenosphere to LM13 aluminum alloy and investigated it for dry sliding wear behavior. It was observed that the size of the cenosphere affects the wear behavior of the material. As cenosphere size decreases, wear resistance increases. The study shows that the abrasive mechanism is a dominating factor. V. Manakeri et al. [19] checked the wear behavior of magnesium/glass micro-balloon incorporated syntactic foam in dry sliding conditions. It was found that abrasion and oxidation were the prominent mechanisms behind wear. S. Kumar and O. P. Pandey [20] prepared close-cell metal foam of LM-13 alloy through the melt route method. The samples were tested on pin-on-disc apparatus at room temperature. In the study, the load varied from 9.8 to 29.4 N under dry sliding wear conditions. The study concludes that the wear rate depends upon the cell size and cell wall thickness of the foam. H. Sharifi et al. [21] prepared an open-cell metal foam with Al-Mg/Al<sub>2</sub>O<sub>3</sub> and Al-Mg/Al<sub>2</sub>O<sub>3</sub>-SiC. Using a pin-on-disc machine, wear tests were done. The results showed that material wear depends on their PPI (pores per inch), cell size, density, and the load put on them.

Furthermore, different authors investigated and assessed the friction and wear properties of pure aluminum and its alloys. The friction and wear behavior of pure Al and Al 6061 with surface porosity was investigated by A. Sinha et al. [22]. The samples were tested under low load conditions (1.5, 2, 2.5, 3, 4, and

5 N) at 600 rpm. For pure Al and Al 6061, the wear rate increases with increasing porosity as the load increases, and a similar pattern was found with increasing sliding distance. With the inclusion of graphite and SiC particles, Parmeshwar P. Ritapure et al. [23] developed an Al-25Zn alloy-based hybrid composite. An essential facet for wear was applied load, followed by sliding speed.

In recent decades, numerous works have been reported on the wear study of composite material, pure metals, alloys, open-cell metal foam, etc. Since close cell, metal foam engenders the place as a structural material due to its fascinating property. It has become necessary to understand the wear behavior of Al-based close metal foam to find practicality in lightweight structures where sliding wear plays a significant role. This research aims to understand better the dry sliding wear behavior of aluminum metal foam reinforced with Zn at weight percentages of 0, 0.5, and 1 %.

## 2. Experimental procedure

### 2.1. Material and method

In this study, pure aluminum ingots were taken as parent metal, Ca granules (2 wt.%) were taken as a thickening agent, and CaCO<sub>3</sub> (1 wt.%) as a blowing agent to prepare metal foam through the melt route method. Pure zinc has been taken as reinforcement in this study. The materials for the experiments were purchased from Gayatri Industries, Roorkee, Uttarakhand, India. Samples were prepared in a pit furnace equipped with stirring arrangements.

Figure 1 represents the fabrication procedure of metal foam. In the process, initially, aluminum metal was melted in a graphite crucible at about 660 °C. Afterward, the thickening agent was added to the melt and mixed homogeneously with the help of a stirrer at about 300 rpm. The next step was the addition of Zn particles, followed by adding CaCO<sub>3</sub> as a blowing agent. During this step, the temperature was maintained at 680 ± 10 °C, and the melt was stirred at 500 rpm.

The mixture was stirred thoroughly for about 5 min and then left for foaming. Later, the crucible was removed and placed in an open atmosphere to cool in still air. The detailed composition and designation are given in Table 1.

## 3. Characterization

### 3.1. Physical characterization

The samples were covered with a light polymer film to prevent them from water penetration. Archimedes'

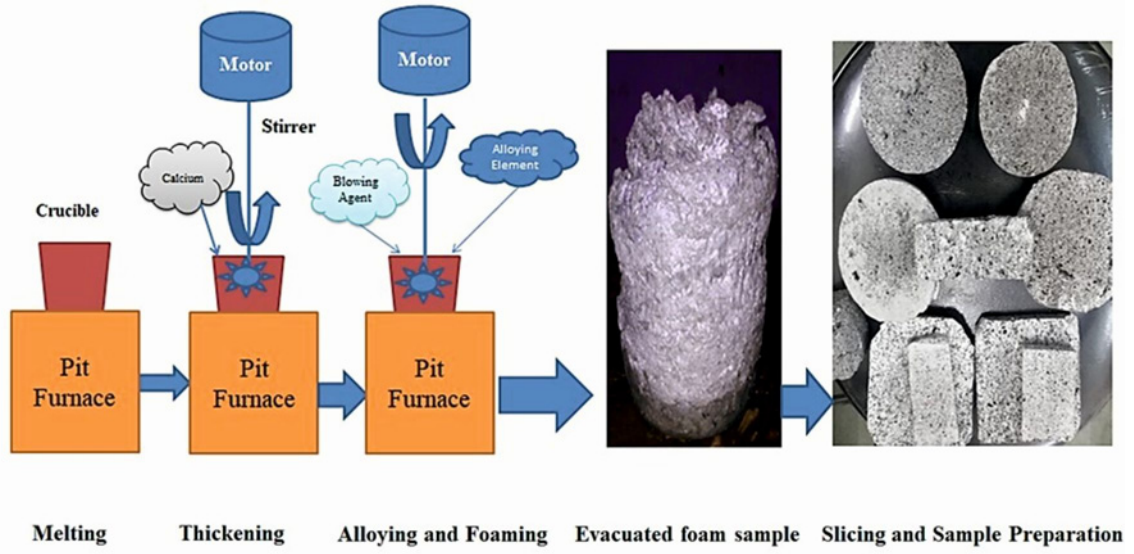


Fig. 1. Schematic diagram representing fabrication of foam.

Table 1. Detailed composition and designation of prepared samples

Designation	Density ( $\text{g cm}^{-3}$ )	Porosity (%)	Average pore size (mm)
Foam-A	0.67	75	2–4
Foam-B	0.7692	71	2–5
Foam-C	0.3946	85	1–3

principle was used for measuring the density of prepared samples. The porosity of foams in percentage was calculated by the given formula:

$$\text{Percentage of porosity} = \frac{\rho_{\text{al}} - \rho_{\text{foam}}}{\rho_{\text{al}}}, \quad (1)$$

where  $\rho$  represents density in  $\text{g cm}^{-3}$ . The fabricated metallic foam samples' macrostructure evaluation was carried out using a digital camera of the good pixel. The photos were taken of specimens to check the pore size, irregularity of pores, and distribution of pores. The size of pores was determined theoretically by the given formula:

$$D = L/0.616, \quad (2)$$

where  $D$  represents the average diameter of pores (mm), and  $L$  represents the average chord length of pores (mm).

### 3.2. Wear characterization

The samples were tested on a pin-on-disc sliding wear apparatus (Ducom Pin-on-Disc rig) under dry

conditions at room temperature as per ASTM G99. The samples were cut into  $8 \times 8 \times 35 \text{ mm}^3$  cuboids for wear tests. The samples were tested on a 10 cm track diameter of stainless steel disc, rotating at a constant sliding speed of  $2.5 \text{ m s}^{-1}$ . The varying parameters for the study are load (5, 10, 15, and 20 N) and distance (1000, 2000, 3000, and 4000 m). All the samples were weighed before and after testing in the digital weighing machine with 0.1 mg precision. The specific wear rate (SWR) for the specimens was calculated by the given formula:

$$\text{SWR} = \frac{m_1 - m_2}{\rho l f_n}, \quad (3)$$

where SWR is the specific wear rate in  $(\text{mm}^3 \text{ N}^{-1} \text{ m}^{-1})$ ,  $m_1$  and  $m_2$  are initial and final masses (g),  $\rho$  is the density ( $\text{g cm}^{-3}$ ),  $l$  is the sliding distance (m), and  $f_n$  is the load applied (N).

The samples were carefully cleaned with distilled water and then left for drying inside the room. To understand the mechanism behind wear SEM, images of samples were obtained through scanning electron microscopy (SEM, ZEISS EVO-18).

## 4. Results and discussion

### 4.1. Morphology of produced foams

Figure 2a illustrates the optical image of Foam-A. In most of the area, the pores appear almost equal in size, but there are also some large pores. The average size of pores varies between 2–4 mm. Figure 3a represents the SEM image of Foam-A in which some large pores can be depicted clearly. Figure 2b shows a cross-section image of Foam-B, which has the high-

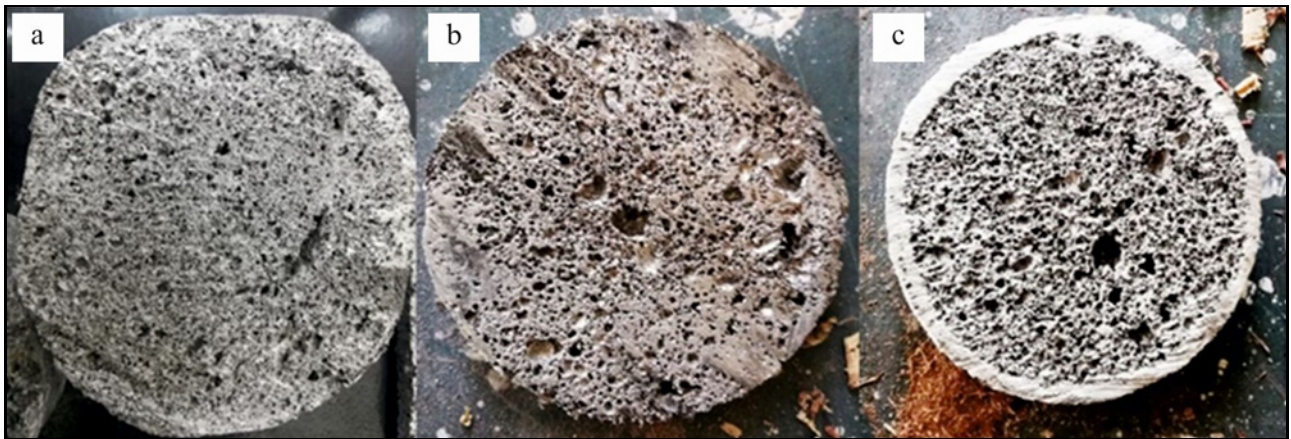


Fig. 2. Optical images of (a) Foam-A, (b) Foam-B, and (c) Foam-C.

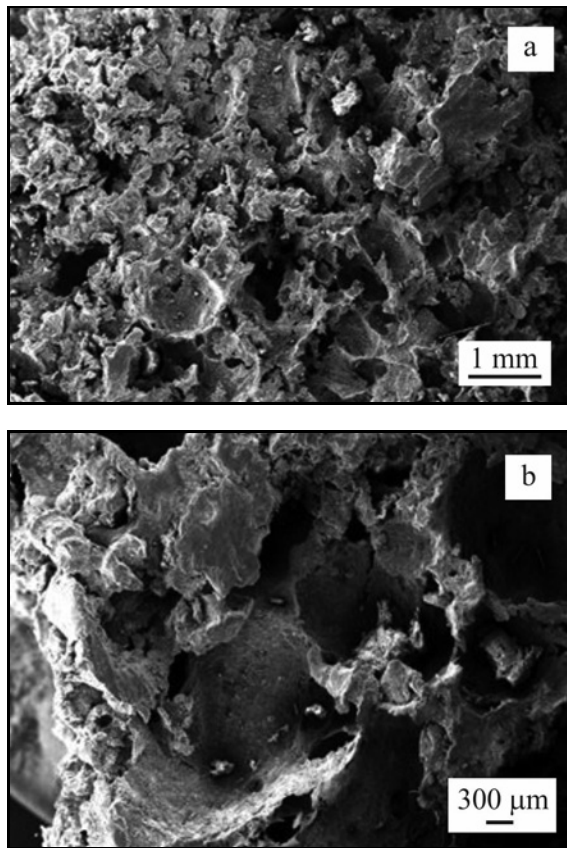


Fig. 3. SEM image of (a) Foam-A and (b) Foam-B.

est irregularity and non-uniformity in pore formation. The non-uniformity can also be seen in the Foam-B SEM image, which is represented in Fig. 3b. These are the consequences of unstable bubble formation. As the plateau border thickness reduces, the borders cannot bear the pressure obtained inside the bubbles, which finally breaks the cell wall, and the bubble enlarges. To prevent bubble enlargement inside the foam, the thickening agent plays a significant role in averting

Table 2. Designation and physical characterization of the foams

Designation	Composition (wt.%)	
	Al	Zn
Foam-A	100	0
Foam-B	99.5	0.5
Foam-C	99	1

the conversion, coalescence, and coarsening process in bubble formation [8]. The size of the pores ranges from 2 to 5 mm. In Fig. 2c, the pores are distributed uniformly and are of uniform size. Albeit some of the large pores are visible, the pores still look regular, thoroughly developed, and uniform. Figures 4a–c illustrate the EDX, SEM image, and composition distribution of Foam-C. The figures show that zinc is uniformly distributed throughout the matrix at a concentration of almost 1 wt.%. The average pore size varies between 1 to 3 mm. Foam-C has a density of about  $0.394 \text{ g cm}^{-3}$  and a relative density of about 15%, indicating that the foam expands significantly. The summary of the physical properties of the foams is tabulated in Table 2.

## 4.2. Sliding wear properties

### 4.2.1. Based on constant sliding distance (2000 m)

The samples were tested at a sliding distance of 2000 m, with all other variables held constant. The load varied from 5 to 20 N in this study. The graph in Fig. 5a shows that the specific wear rate (SWR) increases for all samples with an increase in load. This is because mechanical locking between the samples and tool increases with an increase in load, which increases the material removal rate.

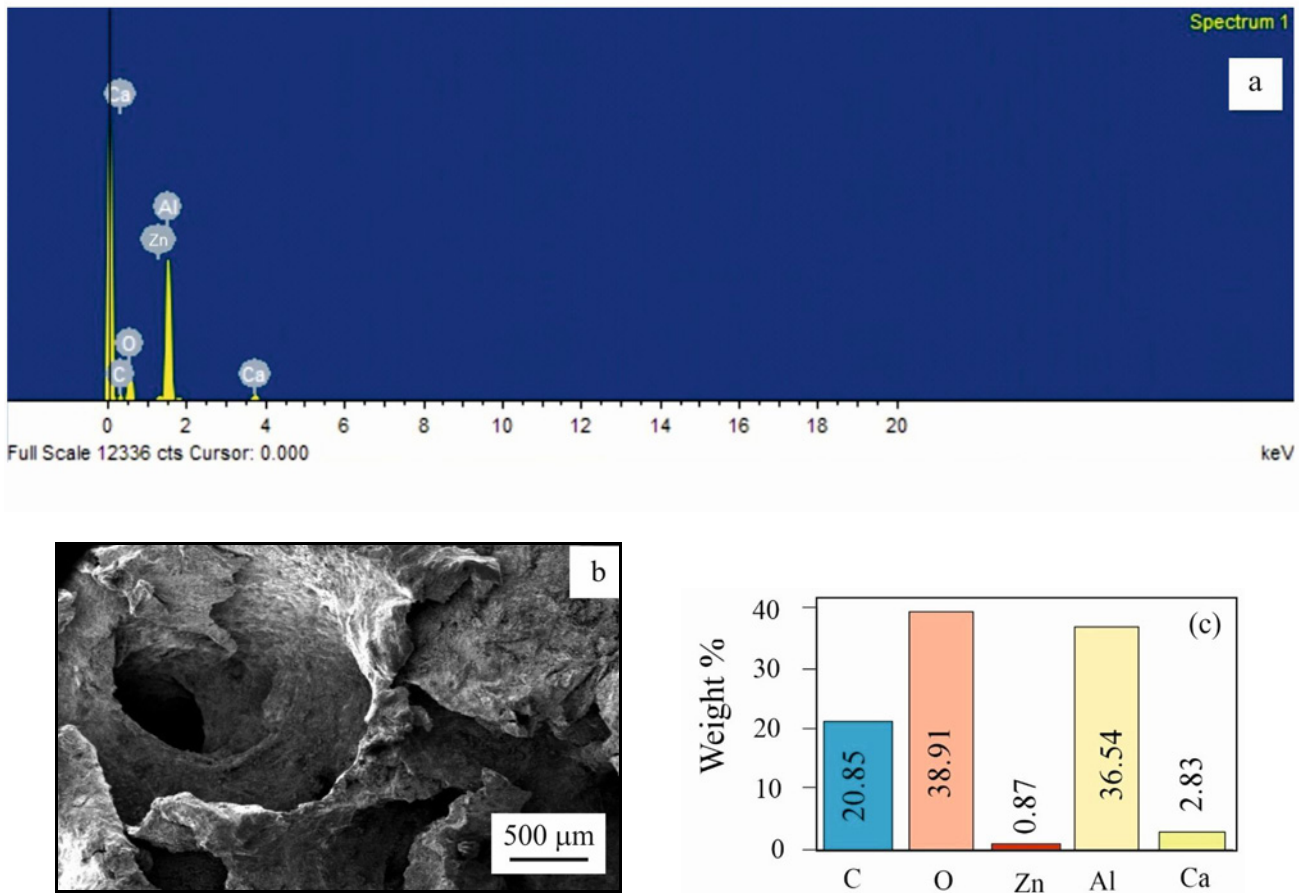


Fig. 4. (a) EDX, (b) SEM image, and (c) composition distribution of Foam-C.

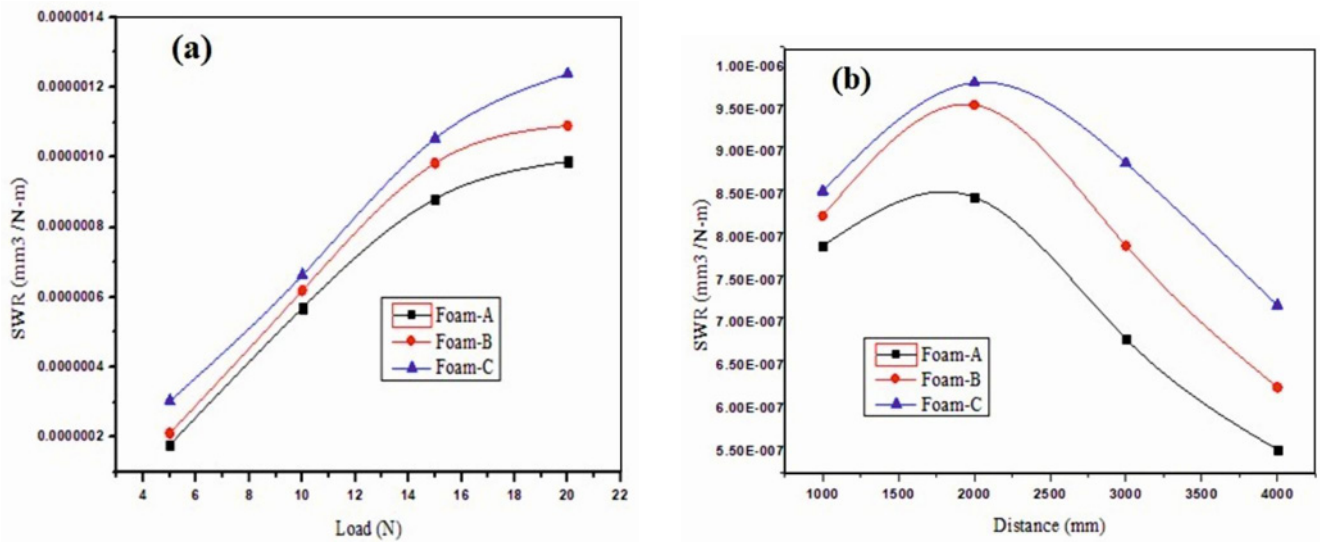


Fig. 5. (a) SWR vs. load curve for constant sliding distance condition (2000 m) and (b) SWR vs. distance curve for constant load condition (15 N).

It is worth noting that with the escalation in the percentage of Zn particles in the metallic foam, the SWR of the samples increases, which is contradictory behavior as reported in previous studies. Look-

ing at morphology and porosity, it is discovered that porosity is maximum for Foam-C and minimum for Foam-B, which helps understand the inconsistent behavior. Moreover, Foam-C has the highest porosity,

and porosity adversely affects the wear resistance [24].

#### 4.2.2. Based on constant load (15 N)

Figure 5b shows the relation between varying sliding distances (1000, 2000, 3000, and 4000 m) and SWR at constant load conditions. For this study, the value of the load is taken at 15 N. The curve shows the increment in SWR for foam samples before 2000 m and then shows a small steady region where SWR almost becomes constant, and afterward, it falls steeply. The increasing state can be defined as the transition stage and the constant state as the steady stage. A significant weight loss is observed at the start of sliding, which decreases after the steady-state value. This term of significant weight loss is known as Run-in and is found in all machines. At the start, it is observed that there are some already deformed asperities or some material build-up edge on the wear track that forms wear particles. As original asperities form and separate, a smooth wear track in the soft material will be observed in the sliding direction. During this period, some subsurface voids begin to form. As the sliding progresses, the subsurface voids reach up-to-critical length, and shearing on the surface starts, leading to the beginning of the catastrophic wear regime [11]. After achieving a steady state, the SWR of all prepared foams decreases. According to Sasada et al. [25, 26], oxidation of both surfaces occurs after the particles are transferred from the opposite contacting surfaces, which helps to minimize the wear rate.

#### 4.3. Effect of porosity on sliding wear

Figure 6a shows the relationship between SWR and foam porosity under a constant load of 15 N and varying sliding distances. The trend can be observed that at 2000 m, all the foams show the highest SWR and decreases afterward for subsequent distances. SWR vs. porosity is depicted in Fig. 6b at a constant distance of 2000 m and under varying load conditions. It can be observed that SWR increases with load for all the samples. Gui et al. [27] represented the pores as a source of cracks initiated by an applied force. High porosity leads to low strength and a high wear rate. Foam-C has the highest porosity as well as the highest SWR, validating prior research.

Foam-A shows the lowest SWR among all the foams, with higher porosity than Foam-B. The experimental findings contradict previous research that indicates SWR increases as porosity increases. Even though Foam-A and Foam-B have similar porosities, Foam-B's sliding wear resistance experiences a rise, probably due to irregularity and non-uniformity in pore formation. Deshpande and Lin [28] suggested a similar pattern that depending on the pore geometry

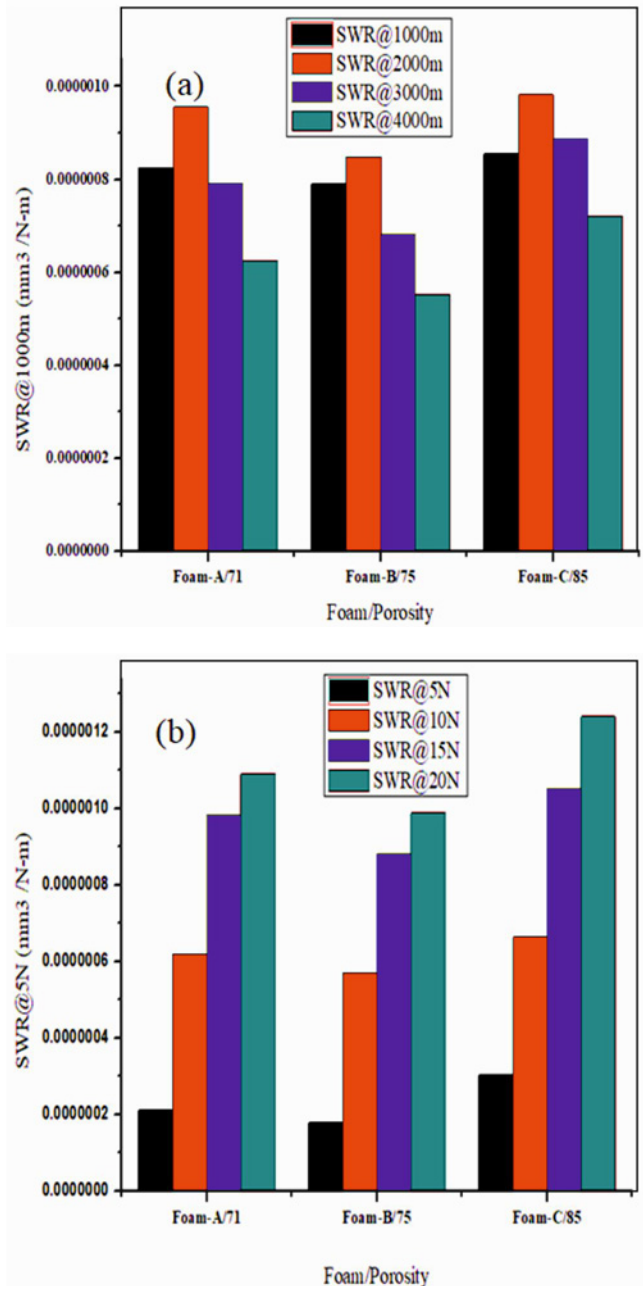


Fig. 6. (a) SWR vs. porosity of Al/Zn foam at a varying distance and constant load of 15 N. (b) SWR vs. porosity of Al/Zn foam at varying load and constant sliding distance of 2000 m.

and distribution, wear resistance can vary, giving authentication towards experimental findings. It is concluded from empirical results that the value of SWR in foams is affected by porosity and cell wall geometric properties.

#### 4.4. Mechanism of wear

The foam with the highest SWR is being studied to understand the mechanism behind foam wear.

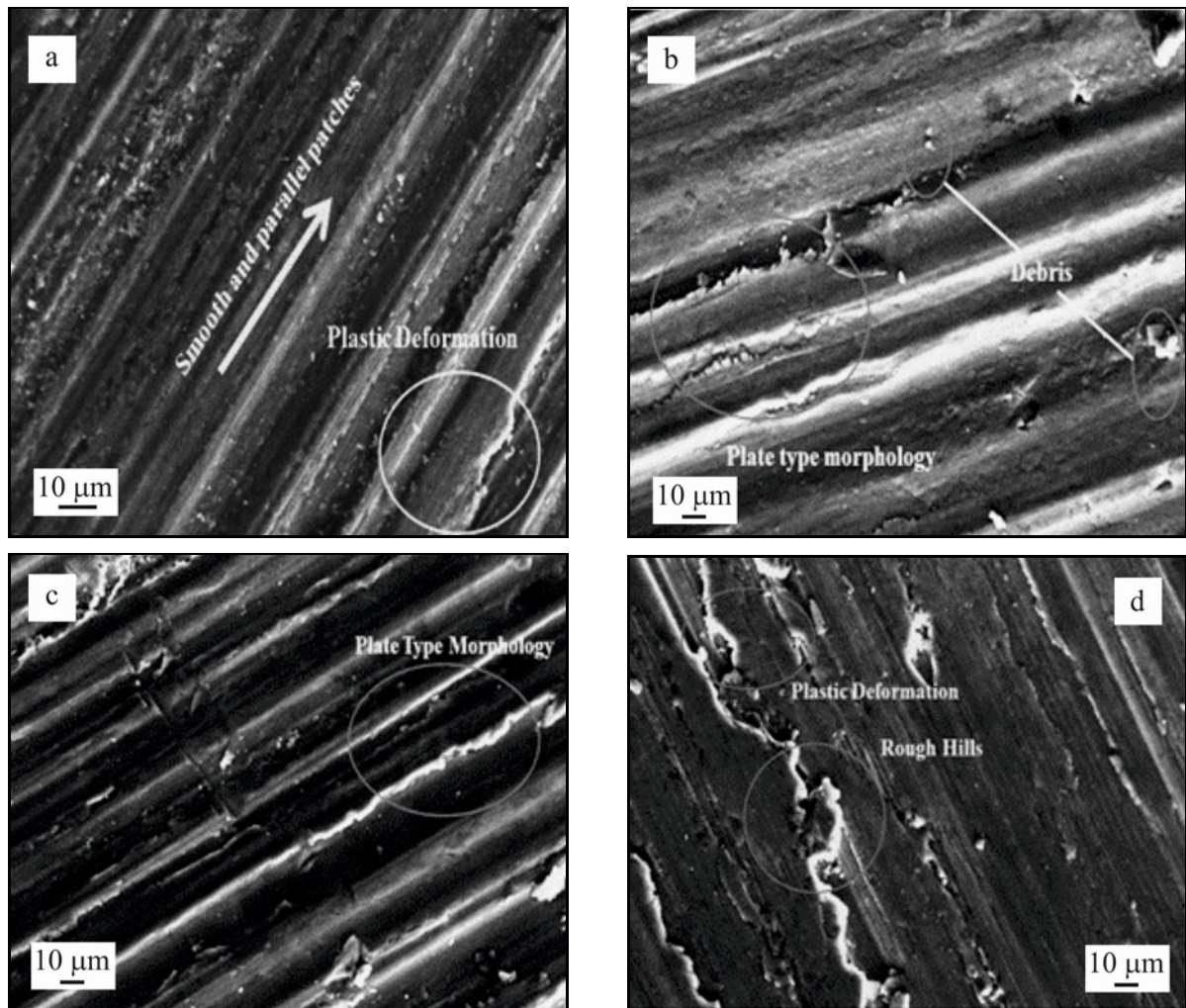


Fig. 7. SEM image of (a) Foam-C at 5 N, (b) Foam-C at 10 N, (c) Foam-C at 15 N, and (d) Foam-C at 20 N.

The study uses Foam-C with varying load conditions and a constant sliding distance of 2000 m. Figure 7a depicts an SEM image of Foam-C with an extended sliding track at 5 N and 2000 m. The patches found are not too deep due to the low applied load of 5 N. Under normal contact force, the hard asperities penetrate the softer surface as wear initiates. As sliding progresses, a tangential motion removes the softer material by micro-plowing, micro-cutting, and micro-cracking [27]. Consequently, the worn surface is represented as grooves and rough scratches. These are the combined effects of two-body abrasive wear. Researchers [21, 22] reported a similar wear mechanism at lower load conditions.

The study of Foam-C at 10 N load and 2000 m in Fig. 6b shows plastic deformation and the elimination of grooves: as the load increases, normal contact force on the surface increases. The surface can be classified into two parts based on the distance from the slider: the surface and the subsurface. The surface is the closest to the slider, while the subsurface is the farthest. The dislocations at the surface will start pil-

ing up as the sliding progresses, so it will be unable to perform any cold work, resulting in the growth of fatigue cracks and, after that, joining, leading towards significant plastic deformation [21, 29]. As a result, the formation of dislocations in the material, leading to plastic deformation, points towards delamination theory. Figure 7b also shows some debris particles, which can be loose or embedded in the soft matrix, but with an increase in applied load, they can crush and form a film between contacting surfaces [30].

More rupture is observed in Fig. 7c at 15 N load and 2000 m representing plastic deformation. The grooves deformed plastically and had become almost smooth with an increase in load. Due to the increased load, plastic deformation and intermetallic adhesion occurred, creating cold weld junctions between the contacting surfaces. As the sliding continues, tearing occurs within the surface, resulting in a plate-like morphology, and adhesion wear is depicted in this way. The part with fewer connections with the slider still represents flat lines, indicating that abrasion is also prominent in this area.

Figure 7d shows the SEM image at 20 N load and 2000 m, with deeper grooves, surface rupture, and plastic deformations. Since the load, in this case, is 20 N, deeper grooves are visible, and material is piled up mainly from the material's surface. Rough hills can also be seen around the contact area, which occur due to the plastic flow of the material. Plastic deformation in the surface indicates severe wear due to high shearing forces and metal softening due to temperature rise [31]. So, the dominating factor, in this case, is plastic flow and delamination.

## 5. Conclusions

Through the melt route method, aluminum metal foams containing Zn (0, 0.5, and 1 wt.%) as an alloying element were successfully fabricated. The samples were analyzed for dry sliding wear behavior on the pin-on-disc equipment. For experimental findings, load and distance were varied while sliding speed and track diameter were constrained. The vital research findings are summarized below:

- SWR increases with an increase in load for all the samples at constant sliding distance conditions.
- SWR is highest at 2000 m for all the cases of foams at constant load conditions.
- SWR is minimum for Foam-A and maximum for Foam-C for constant load and distance conditions.
- With the addition of Zn in the melt, SWR increases. SWR depends upon the porosity as well as on the cell wall geometry. It can be concluded that SWR strongly depends upon the cell wall properties rather than the addition of reinforcing elements.
- At lower load conditions, the wear mechanism is abrasion which occurs due to contact with asperities of different hardness.
- The mechanism transfers from abrasion to plastic flow and delamination at higher load conditions.

## References

- [1] J. Banhart, Aluminum foams: On the road to real applications, *MRS Bulletin* 28 (2003) 290–295. <https://doi.org/10.1557/mrs2003.83>
- [2] J. Banhart, Aluminum foam technology – towards industrial implementation, *Indian Foundry Journal* 51 (2005) 36–41.
- [3] J. Banhart, Light-metal foams – History of innovation and technological challenges, *Advanced Engineering Materials* 15 (2013) 82–111. <https://doi.org/10.1002/adem.201200217>
- [4] A. Bisht, B. Gangil, V. K. Patel, Selection of blowing agent for metal foam production: A review, *Journal of Metals, Materials and Minerals* 30 (2020) 1–10. <https://doi.org/10.55713/jmmm.v30i1.597>
- [5] K. V. Steiner, J. Banhart, J. Baumeister, M. Weber, Production and properties of ultra-lightweight aluminum foams for industrial applications, In: *Proceeding of the 4th International Conference on Composites Engineering* (1997), Big Island of Hawaii, pp. 943–944.
- [6] J. Banhart, Manufacture, characterization and application of cellular metals and metal foams, *Progress in Materials Science* 46 (2001) 559–632. [https://doi.org/10.1016/S0079-6425\(00\)00002-5](https://doi.org/10.1016/S0079-6425(00)00002-5)
- [7] F. Baumgärtner, I. Duarte, J. Banhart, Industrialization of powder compact foaming process, *Advanced Engineering Materials* 2 (2000) 168–174. [https://doi.org/10.1002/\(SICI\)1527-2648\(200004\)2:4%3C168::AID-ADEM168%3E3.0.CO;2-O](https://doi.org/10.1002/(SICI)1527-2648(200004)2:4%3C168::AID-ADEM168%3E3.0.CO;2-O)
- [8] A. Bisht, B. Gangil, Structural and physico-mechanical characterization of closed-cell aluminum foams with different zinc additions, *Science and Engineering of Composite Materials* 25 (2018) 789–795. <https://doi.org/10.1515/secm-2016-0307>
- [9] A. Mirzaei-Solhi, J. Khalil-Allafi, M. Yusefi, M. Yazdani, A. Mohammadzadeh, Fabrication of aluminum foams by using CaCO<sub>3</sub> foaming agent, *Materials Research Express* 5 (2018) 096526. <https://doi.org/10.1088/2053-1591/aad88a>
- [10] T. Shi, X. Chen, Y. Cheng, Y. Liu, H. Zhang, Y. Li, Microstructure and compressive properties of aluminum foams made by 6063 aluminum alloy and pure aluminum, *Materials Transactions* 59 (2018) 625–633. <https://doi.org/10.2320/matertrans.M2017300>
- [11] M. H. Ghaleh, N. Ehsani, H. R. Baharvandi, High-porosity closed-cell aluminum foams produced by melting method without stabilizer particles, *International Journal of Metalcasting* 15 (2021) 899–905. <https://doi.org/10.1007/s40962-020-00528-w>
- [12] D. Yang, Z. Zhang, X. Chen, X. Han, T. Xu, X. Li, J. Ding, H. Liu, X. Xia, Y. Gao, Y. Wang, Quasi-static compression deformation and energy absorption characteristics of basalt fiber-containing closed-cell aluminum foam, *Metals* 10 (2020) 921. <https://doi.org/10.3390/met10070921>
- [13] G. Timac, H. O. Gulsoy, Ni-718 superalloy foam processed by powder space-holder technique: Microstructural and mechanical characterization, *Kovove Mater.* 55 (2017) 273–278. [http://dx.doi.org/10.4149/km\\_2017\\_4\\_273](http://dx.doi.org/10.4149/km_2017_4_273)
- [14] E. Linul, L. Marşavina, P. A. Linul, J. Kovacic, Cryogenic and high temperature compressive properties of metal foam matrix composites, *Composite Structures* 209 (2019) 490–498. <https://doi.org/10.1016/j.compstruct.2018.11.006>
- [15] J. Kováčik, F. Šimančík, Comparison of zinc and aluminum foam behaviour, *Kovove Mater.* 42 (2004) 79–90.
- [16] X. Xia, X. Chen, Z. Zhang, X. Chen, W. Zhao, B. Liao, B. Hur, Compressive properties of closed-cell aluminum foams with different contents of ceramic microspheres, *Materials & Design* 56 (2014) 353–358. <https://doi.org/10.1016/j.matdes.2013.11.040>
- [17] A. Bisht, B. Gangil, V. K. Patel, Physico-compression, sliding wear and energy absorption properties of Zn/Mg infiltrated closed cell aluminum foam, *Materials Research Express* 6 (2019) 106583. <https://doi.org/10.1088/2053-1591/ab3b80>
- [18] A. Vishwakarma, D. P. Mondal, S. Birla, S. Das, N. Prasanth, Effect of cenosphere size on the dry sliding

- wear behaviour LM13-cenosphere syntactic foam, Tribology International 110 (2017) 8–22.  
<https://doi.org/10.1016/j.triboint.2017.01.041>
- [19] V. Manakari, G. Parande, M. Doddamani, M. Gupta, Evaluation of wear resistance of magnesium/glass microballoon syntactic foams for engineering/biomedical applications, Ceramics International 45 (2019) 9302–9305.  
<https://doi.org/10.1016/j.ceramint.2019.01.207>.
- [20] S. Kumar, O. P. Pandey, Study of microstructure and mechanical properties of particulate reinforced aluminum matrix composite foam. In: T. Sano, T. S. Srivatsan (Eds.), Advanced Composites for Aerospace, Marine, and Land Applications II., Springer, 2015, pp. 245–257.  
[https://doi.org/10.1007/978-3-319-48141-8\\_19](https://doi.org/10.1007/978-3-319-48141-8_19)
- [21] H. Sharifi, K. Ostovan, M. Tayebi, A. Rajaei, Dry sliding wear behavior of open-cell Al-Mg/Al<sub>2</sub>O<sub>3</sub> and Al-Mg/SiC-Al<sub>2</sub>O<sub>3</sub> composite preforms produced by a pressureless infiltration technique, Tribology International 116 (2017) 244–255.  
<https://doi.org/10.1016/j.triboint.2017.07.023>.
- [22] A. Sinha, Z. Farhat, Effect of surface porosity on tribological properties of sintered pure Al and Al 6061, Materials Sciences and Applications 6 (2015) 549–566.  
<http://dx.doi.org/10.4236/msa.2015.66059>
- [23] P. P. Ritapure, Y. R. Kharde, R. G. Yadav, S. Y. Pawar, Influence of SiC on solid particle erosion and mechanical behaviour of Al-25Zn alloy based novel metal matrix composites fabricated through stir casting technique, Advances in Materials and Processing Technologies 28 (2021) 1–5.  
<https://doi.org/10.1080/2374068X.2021.1970987>
- [24] D. Cree, M. Pugh, Dry wear and friction properties of an A356/SiC foam interpenetrating phase composite, Wear 272 (2011) 88–96.  
<https://doi.org/10.1016/j.wear.2011.07.008>
- [25] T. Sasada, Wear research in Japan: Trends and future directions, Wear 100 (1984) 561–577.  
[https://doi.org/10.1016/0043-1648\(84\)90033-4](https://doi.org/10.1016/0043-1648(84)90033-4)
- [26] T. Sasada, S. Ban, S. Norose, T. Nakano, Wear of binary alloys – difference in wear mode between solid solutions and intermetallic compounds, Wear 159 (1992) 191–199.  
[https://doi.org/10.1016/0043-1648\(92\)90302-O](https://doi.org/10.1016/0043-1648(92)90302-O)
- [27] M. Gui, S. B. Kang, J. M. Lee, Influence of porosity on dry sliding wear behavior in spray deposited Al-6Cu-Mn/SiC<sub>p</sub> composite, Materials Science and Engineering A 293 (2000) 146–156.  
[https://doi.org/10.1016/S0921-5093\(00\)01052-2](https://doi.org/10.1016/S0921-5093(00)01052-2)
- [28] P. K. Deshpande, R. Y. Lin, Wear resistance of WC particle reinforced copper matrix composites and the effect of porosity, Materials Science and Engineering A 418 (2006) 137–45.  
<https://doi.org/10.1016/j.msea.2005.11.036>
- [29] N. P. Suh, The delamination theory of wear, Wear 25 (1973) 111–124.  
[https://doi.org/10.1016/0043-1648\(73\)90125-7](https://doi.org/10.1016/0043-1648(73)90125-7)
- [30] A. M. Hassan, A. T. Mayyas, A. Alrashdan, M. T. Hayajneh, Wear behavior of Al-Cu and Al-Cu/SiC components produced by powder metallurgy, Journal of Materials Science 43 (2008) 5368–535.  
<https://doi.org/10.1007/s10853-008-2760-5>
- [31] M. I. Ul Haq, A. Anand, Friction and wear behavior of AA 7075-Si<sub>3</sub>N<sub>4</sub> composites under dry conditions: Effect of sliding speed, Silicon 11 (2019) 1047–1053.  
<https://doi.org/10.1007/s12633-018-9967-0>